Chapter 2

Theoretical Background

This chapter reviews the material properties of $CuInSe_2$ and its alloys. A brief description of the principle of solar cells with simple model (p-n junction), the ideal and illuminated current-voltage characteristics of a solar cell are presented. The solar cell parameters will be defined, and the parameter influencing the conversion efficiencies will finally be outlined.

2.1 Material Properties of $CuIn_{1-x}Ga_xSe_2$ Chalcopyrite Semiconductors

The crystal structure of ternary I-III-VI_2 (I=Cu; III=In,Ga; VI=Se) chalcopyrite compounds such as $CuInSe_2$ is well established to be chalcopyrite at room temperature having the space group symmetry $I\bar{4}2d$ and it transforms to the sphalerite structure at 805°C. They are the structure analogs of II-VI, ZnSe, zinc blende structure as shown in Fig. 2.1 [21]. Therefore, their crystal structures are expected to be similar.

The chalcopyrite unit cell is tetragonal, whereas the zinc blende unit cell is cubic consisting of two interpenetrating face centered cubic sublattices. The two sublattices are displaced by one quarter of a body diagonal, each sublattice having only one type of atoms. These may be considered as a cation (Zn) and an anion (Se) sublattice. In each $CuInSe_2$ unit cell, the anion sublattice is occupied by the Se atoms, while the cation sublattice is shared by the Cu and In atoms. If the Cu and In atoms are randomly distributed in the sublattice, the structure of the compound remains zinc blende. However, if they are ordered as shown in Fig. 2.1, the structure of the compound is chalcopyrite. Hence, each cation Cu and In in the $CuInSe_2$ compound has four Se anions as nearest neighbors. Because of the difference in the strengths

between the Cu-Se and In-Se bonds in the chalcopyrite structure, there are additional noncubic aspects of chalcopyrite structure, i.e., 1) a doubling of the unit cell in the z-direction resulting from an ordering of the two cations, 2) a compression of the crystal lattice along the c-axis as indicated by a tetragonal distortion (2-c/a) and 3) anionic displacements of the anion sites away from the cubic (1/4, 1/4, 1/4) to the tetragonal (0, 1/4, 1/8) position and symmetrically related positions due to the unequal bond lengths between Cu-Se and In-Se ions [22].

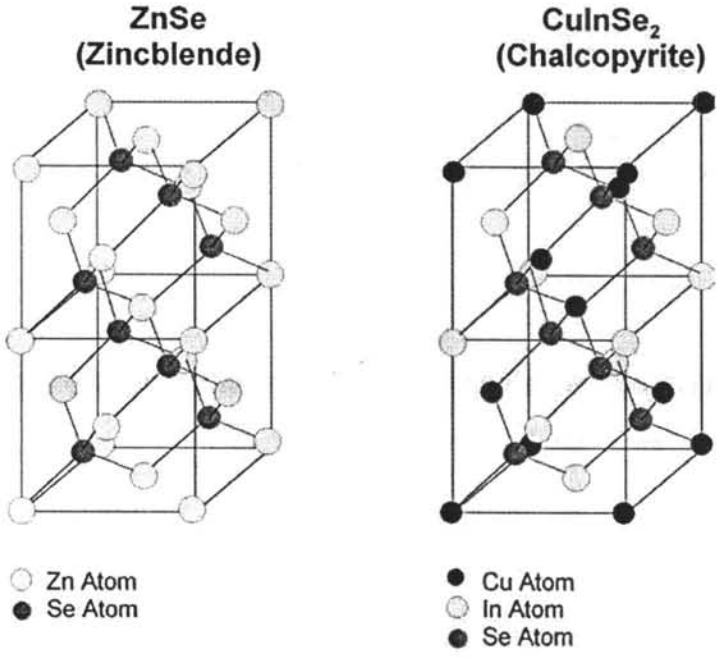

Figure 2.1: Schematic representation of $CuInSe_2$ chalcopyrite structure analogs to ZnSe zinc blende structure [23].

2.1.1 Phase Diagram of Cu-In-Se System

The structural, optical and electrical properties of chalcopyrite thin films are influenced by the presence of secondary phases in the bulk of the material. Phase diagrams are helpful in predicting the existence of different secondary phases in the films. The complex ternary phase diagrams of I-III-VI_2 chalcopyrites can be reduced to simpler pseudo-binary phase diagrams along the I_2VI-III_2VI_3 tie-line. Thus, the phase information for the $CuInSe_2$ material is considered to be the Cu_2Se-In_2Se_3 pseudo-binary phase diagram as shown in Fig. 2.2 [24]. The phase diagram indicates

that the existence range of the chalcopyrite single phase $CuInSe_2$ (α-phase) is limited by the occurrence of the Cu_2Se phase on the Cu-rich side, the occurrence of β-phase on the In-rich side, and the formation of the δ-phase (the sphalerite phase) at high temperature. This existence range is narrow at Cu concentrations between 24.0 and 24.5% at room temperature corresponding to [Cu]/[In] atomic ratio lies between 1.0 and 0.82. Thus, the stoichiometric and the [Cu]/[In] atomic ratios greater than 1.0, the materials are expected to contain α–$CuInSe_2$ and the secondary phase of Cu_2Se.

The Cu-deficient of $CuInSe_2$ ([Cu]/[In] atomic ratio less than 0.82) [25], a number of different phases exist such as β-phase ($CuIn_2Se_{3.5}$, $CuIn_3Se_5$), γ-phase ($CuIn_5Se_8$). β-phase may be called "ordered vacancy compound" (OVC) or "ordered defect compound" (ODC). However, the phase diagrams represent equilibrium conditions, where the different phases are obtained by cooling a melt with a specific composition, i.e., along vertical lines in the diagram. While, thin film growth processes are usually non-equilibrium conditions, reactions in thin film growth process proceeds at constant temperatures (along horizontal lines in the phase diagram) from one composition to another.

Chalcopyrite $CuInSe_2$ thin films for photovoltaic applications have a slightly Cu-poor composition, and a tendency of phase separation in films may be expected after growth process.

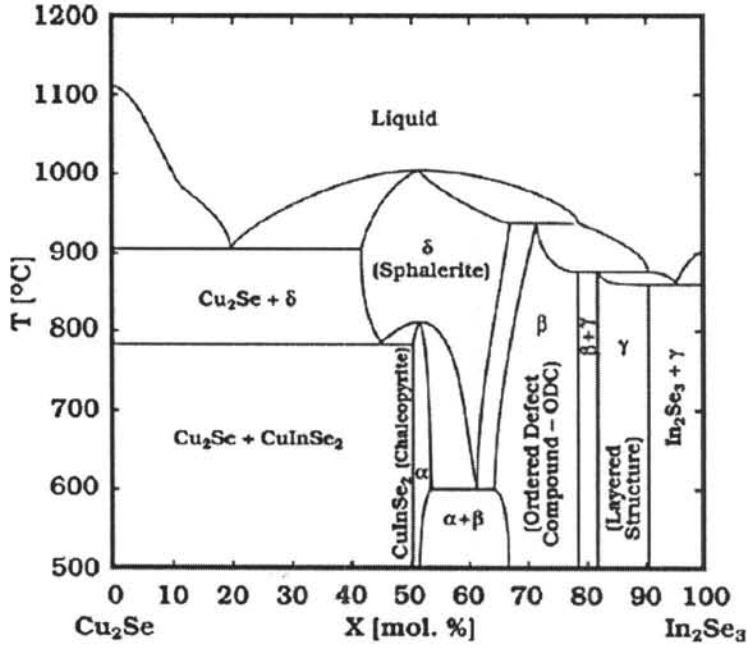

Figure 2.2: Cu_2Se-In_2Se_3 pseudo-binary phase diagram [24].

2.1.2 Phase Diagram of Cu-Ga-Se System

The phase diagram along the Cu_2Se-Ga_2Se_3 pseudo-binary section is shown in Fig. 2.3. $CuGaSe_2$ has also a chalcopyrite structure, the α-phase $CuGaSe_2$ extends further towards Cu-poor compositions (20.7% Cu) than that in the Cu-In-Se system. The existence phases on the Cu-poor side of $CuGaSe_2$ appear to be less complex than that of $CuInSe_2$. These seem to be a few different phases such as $CuGa_3Se_5$, $CuGa_5Se_8$ and Ga_2Se_3 binary phase which has a defect zinc blende (sphalerite) structure. The melting point of $CuGaSe_2$ ($T_m \approx 1080^{\circ}C$) [27] is higher than the melting point of $CuInSe_2$ ($T_m \approx 980^{\circ}C$). Considering the lower value of T_{sub}/T_m ratio for $CuGaSe_2$ than that for $CuInSe_2$ grown at the same temperature, the growth of high-quality $CuGaSe_2$ thin films seems to be more "difficult" than the growth of $CuInSe_2$ films.

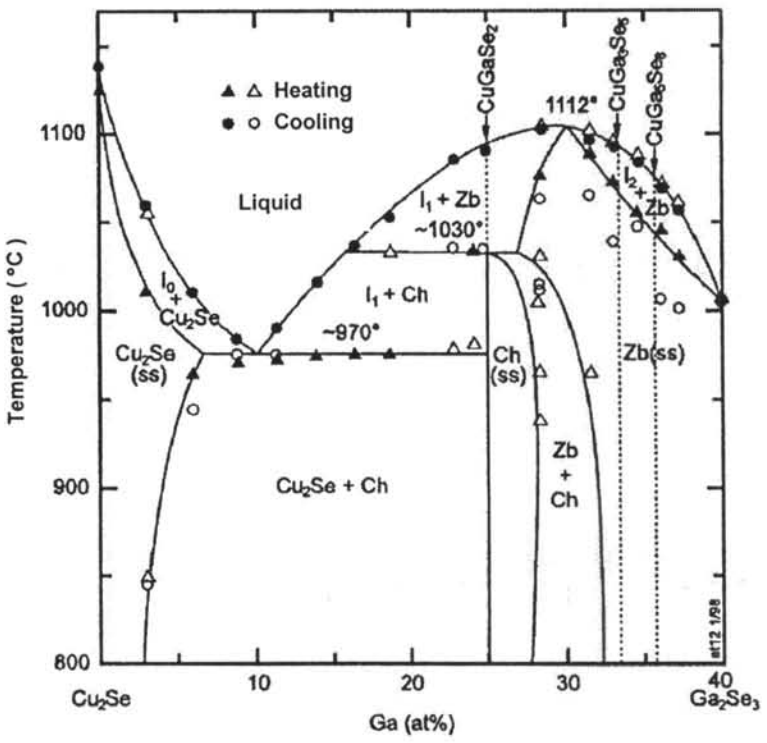

Figure 2.3: Phase diagram along the Cu_2Se-Ga_2Se_3 pseudo-binary section of the Cu-Ga-Se material system [26].

2.2 Defects in $CuInSe_2$

$CuInSe_2$ is a self-doped (intrinsically doped) material. When the compound is formed, it automatically becomes either p- or n-type depending on the composition. The defect chemistry model of $CuInSe_2$ was proposed for its nearly stoichiometric compound by Rincon *et al.* [28]. The deviation of composition from the ideal can be described by two parameters, the molecularity deviation (Δm) and the stoichiometry deviation (ΔS) which are defined as [29, 30]

$$\Delta m = \frac{[Cu]}{[In]} - 1, \tag{2.1}$$

$$\Delta S = \frac{2[Se]}{[Cu] + 3[In]} - 1, \tag{2.2}$$

where [Cu], [In] and [Se] are the total atomic concentrations of Cu, In and Se, respectively in $CuInSe_2$ and [Cu] + [In] + [Se] = 1. In the case of normal $CuInSe_2$, Δm

determines whether there is an excess of Cu_2Se ($\Delta m>0$) or an excess of In_2Se_3 ($\Delta m<0$). ΔS determines whether there is an excess ($\Delta S>0$) or deficiency ($\Delta S<0$) of selenium. These two parameters provide the possibility of major defect pairs as shown in Table 2.1. The defect formation energies are also shown in Table 2.2.

Table 2.1: Majority defect pairs in $CuInSe_2$ under the condition $\Delta m<0$ [28].

Majority defect pair		Stoichiometry deviation (ΔS)
Acceptor	Donor	
V_{Cu}	In_{Cu}	<0
V_{Cu}	V_{Se}	<0
V_{Cu}	In_i	>0
Se_i	In_{Se}	>0
Se_i	In_i	>0

Table 2.2: Formation energies of intrinsic defects in $CuInSe_2$ [28].

Type of defects		Formation energy (eV)
Vacancies	V_{Se}	2.4
	V_{Cu}	2.6
	V_{In}	2.8
Interstitials	Cu_i	4.4
	In_i	9.1
	Se_i	22.4
Antisites	In_{Cu}	1.4
	Cu_{In}	1.5
	In_{Se}	5.0
	Se_{In}	5.5
	Se_{Cu}	7.5
	Cu_{Se}	7.5

The primary intrinsic defects called "native defects" consist of the acceptor type defects and donor-type defects. The acceptor-type defects consist of copper vacancies (V_{Cu}) and copper-on indium antisites (Cu_{In}), while the donor-type defects consist of indium-on copper antisites (In_{Cu}) and selenium vacancies (V_{Se}).

The Cu-rich film ([Cu]/[In] atomic ratio more than 1) is highly conductive because of the presence of highly conductive copper selenide species. This composition is generally p-type because of a large concentration of Cu_{In} defects. The Cu-poor film ([Cu]/[In] atomic ratio less than 1) does not contain copper selenide species. This material can be either n- or p-type. The data from Table 2.2 show that the Cu vacancy defect (V_{Cu}) and the In-on-Cu antisite (In_{Cu}) are the dominant defects in Cu-poor films, which need a smaller energy of formation. The V_{Cu} and In_{Cu} can be attributed to a defect pair ($2V_{Cu} + In_{Cu}$) called the neutral defect complex (NDC). This result is in agreement with those of Zhang *et al.* [31], who proposed that the pairing of defects can change the electrical property in the sample. For example, an isolated V_{Cu} is a shallow acceptor, while an isolated In_{Cu} is a deep donor, but a defect pair based on $2V_{Cu}$ and In_{Cu} is electrically inactive. Therefore, they attributed very efficient self-doping ability of $CuInSe_2$ to the exceptionally low formation energy of Cu vacancies and to the existence of a shallow Cu vacancy acceptor level.

2.3 Band Gap Engineering of Ternary Chalcopyrite Semiconductors

Figure 2.4 shows the energy-band diagram for a $CuGaSe_2$ and $CuInSe_2$ chalcopyrite structure with crystal field and spin-orbit interactions. The valence band maximum at the Brillouin zone center is a triply degenerate state. The perturbation due to the tetragonal crystal field resulting from the change in symmetry from zinc blende to chalcopyrite leads to the nondegenerate states Γ_4 and doubly degenerate Γ_5. The Δ_{cf} changes from positive for $CuInSe_2$ (c/2a = 1.004) to negative for $CuGaSe_2$ (c/2a = 0.9825) [33]. The doubly degenerate Γ_5 is further split by the spin-orbit interaction.

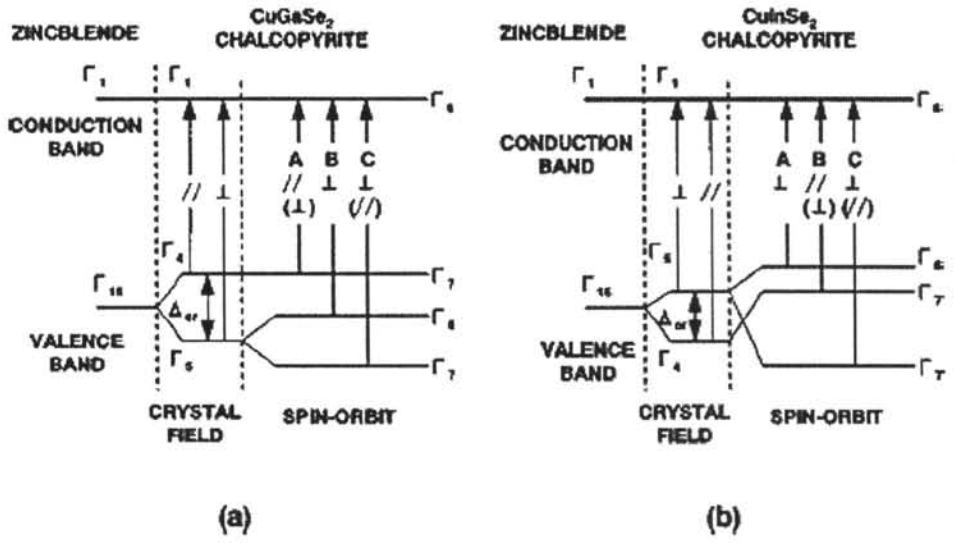

Figure 2.4: Band structure of chalcopyrite type semiconductor (a) $CuGaSe_2$ and (b) $CuInSe_2$. The indications $\perp$ and // show that the transition is allowed for the light polarization E perpendicular and parallel to the crystal axis, respectively. The value Δ_{so} and Δ_{cf} and the spin-orbit are crystal field splittings, respectively [32].

The fundamental transitions from the valence band maximum to the conduction band minimum at the Γ point are shown in Fig 2.4, the symbol $\perp$ and // indicating transitions allows for the light polarization perpendicular or parallel to the crystal axis, respectively. For $CuInSe_2$ chalcopyrite structure (Fig 2.4 (a)) Δ_{cf} is positive and Γ_4 lies below Γ_5. For a $CuGaSe_2$ chalcopyrite structure (Fig 2.4 (b)) Δ_{cf} is negative and Γ_5 lies below Γ_4. This three transitions from the valence bands to the Γ_6 conduction band are referred to as A, B, and C transitions in order of increasing transition energy.

As mentioned in Section 2.1, when In in $CuInSe_2$ is replaced by Ga, the band gap tends to increase. This is an effect of the smaller size of the Ga atom (compared with In), and the various formation energies involved. Some research groups carried out optical absorption measurement to determine the band gap of $CuInSe_2$-$CuGaSe_2$. Albin *et al.* [34] revealed that the band gap of $CuIn_{1-y}Ga_ySe_2$ (y = at% of Ga) varies as

$$E_g = 1.011 + 0.664y - 0.249y(1-y). \quad (2.3)$$

While, Wei *et al.* [35] suggested that Ga incorporation increases the band gap as

$$E_{g,CIGS} = (1-x)E_{g,CIS} + xE_{g,CGS} - bx(1-x),$$

$$E_{g,CIGS} = 1.01(1-x) + 1.65x - 0.15x(1-x), \quad (2.4)$$

where x = [Ga]/([In]+[Ga]), b is the bowing parameter providing the deviation from a linear relationship.

2.4 Principle of Solar Cells

2.4.1 Solar Spectrum

The simple model to determine energy distribution from sunlight assumes that the sun behaves as a black body whose surface is maintained at T = 6000K. Integration over wavelengths yields the solar constant, 1353 W/m^2 [36]. However, the spectral distribution is changed considerably when the sunlight penetrates through the earth's atmosphere. Even for a clear sky the light intensity is attenuated by at least 30%. The degree of attenuation is highly variable due to the changing position of the sun and the change of the light path through the atmosphere. These effects are described by defining an air mass number (AM). The air mass according to IEEE Standard Dictionary of Electrical and Electronics Terms is the mass of air between the Earth's surface and the sun that affects the spectral distribution and intensity of sunlight. AM0 is the spectral distribution and intensity of sunlight outside the Earth's atmosphere. AM1 is the spectral distribution and intensity of sunlight on earth at sea level with the sun directly overhead and a standard atmosphere. When the sun is at an angle θ to overhead, the air mass is given by

$$\text{Air mass} = \frac{1}{\cos\theta}. \quad (2.5)$$

The most widely used is the AM1.5 spectral distribution at ground level when the sun is 45° above the horizon.

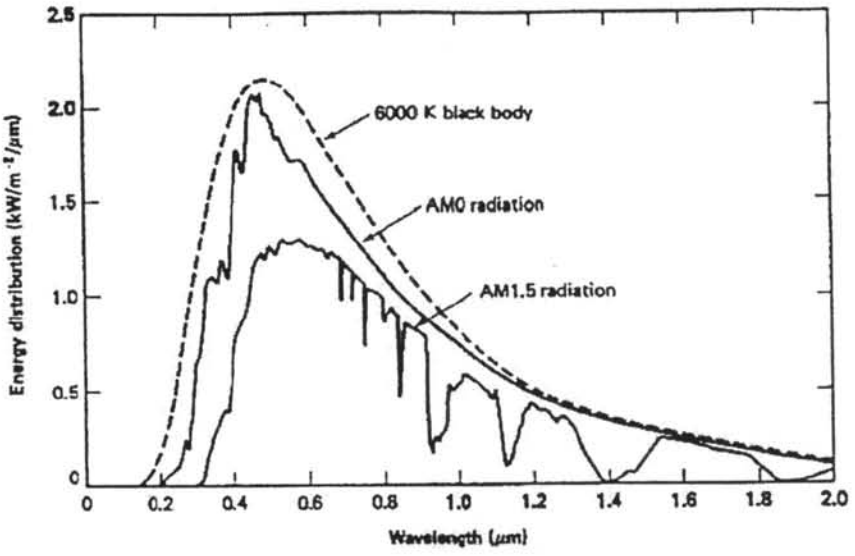

Figure 2.5: Spectral distribution of sunlight. The dashed line indicates the radiation distribution expected from the sun if it were a black body at a temperature of 6000K [37].

2.4.2 Electrical Properties of Solar Cells

Solar cells, or photovoltaic devices, are devices that convert sunlight directly into electricity. The structure is basically a p-n junction diode. The p-n junction is classified into homojunctions and heterojunctions according to whether the semiconductor material on one side of the junction is the same as or different from the other side. When the junction is illuminated, the absorber layer absorbs the photons which their energy is larger than the band gap of the absorber material. The absorbed photons generate electron-hole pairs called photogenerated electron-hole pairs. These photogenerated electron-hole pairs are separated by the internal electric field called "built-in potential" of the junction. The field is created either by a p-n junction within the absorber layer or between the absorber layer and another layer. Typically, solar cell is designed in such a way that after these carriers are swept across the junction, they are collected by the metallic contact. Holes drift to one electrode and electrons drift to the other one. Thus, phenomenon of solar energy conversion involves the process of absorption of radiation, generation of carriers, transportation of carriers to

the junction, separation of the carriers at the junction, collection of the separated carriers and finally generation of power output of the cell.

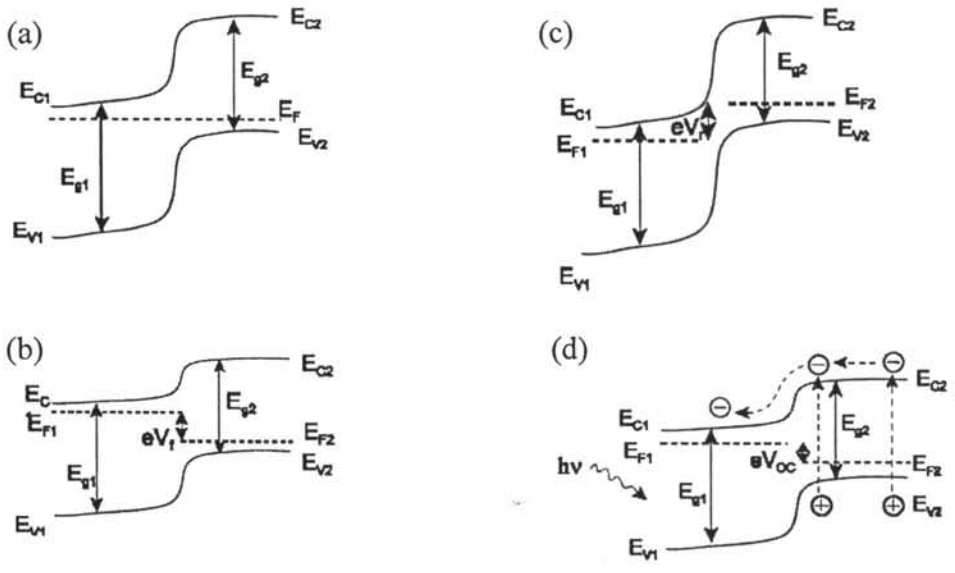

Figure 2.6: A simplified energy band diagram of p-n heterojunction solar cell (a) at thermal equilibrium in dark (b) under forward bias (c) under a reverse bias and (d) under illumination, open circuit conditions. No 1 and 2 in the Figure refer n-type and p-type semiconductor, respectively.

From Fig. 2.6 (a) in the absence of an applied voltage, the Fermi levels of the semiconductors coincide, and there is no current flow. Under forward bias condition, the bias voltage (V_f) shifts the Fermi level of the n-type upwards and that of the p-type downwards, thus lowering the potential energy barrier of the junction, and facilitating the current flow across it. Under reverse bias, the bias voltage (V_r) increases the potential barrier and impedes the current flow. While the junction is under illumination condition, the electron-hole pairs are generated causing an increase in the minority carrier concentration. The potential barrier decreases, allowing the current to flow, and a photovoltage V_{OC} (photovoltage under open circuit conditions, or open circuit voltage) is generated across the junction.

The current transport across the p-n junction is characterized to two currents. The first is the drift current caused by the electrical field in space charge region of the

junction. Second is the diffusion current which flows in the opposite direction and is driven by the concentration gradient of the charge carriers across the junction. The current-voltage (I-V) characteristics of an ideal p-n junction diode in the dark can be described by an expression found by Shockley, called "ideal-diode equation" [38]:

$$I = I_0\left[e^{\frac{qV}{AkT}} - 1\right], \tag{2.6}$$

where I is the diode current, V is the applied bias voltage, I_0 is the leakage current or called "saturation current", q the electron charge. A is the diode ideality factor, k is the Boltzmann constant, T is the absolute temperature.

2.4.3 Current-Voltage Characteristics

The current-voltage (I-V) relation of typical solar cell under illumination, Eq. 2.6 becomes

$$I = I_0\left[e^{\frac{q(V-R_SI)}{AkT}} - 1\right] + \frac{V - R_SI}{R_{SH}} - I_L, \tag{2.7}$$

where R_S and R_{SH} are the series and shunt resistances, respectively. I_L is the light-generated current. From Eq. 2.7, we can determine three important solar cell parameters that are usually used to describe the performance of the cell. The first is the short circuit current (I_{SC}), which represents the current flowing through cell in short circuit condition (V=0). The expression can be written as

$$I_{SC} = I_L - I_0\left[e^{\frac{qR_SI_{SC}}{AkT}} - 1\right] - \frac{R_SI_{SC}}{R_{SH}}. \tag{2.8}$$

Under normal conditions where R_S is small, R_{SH} is large and $I_L >> I_0$, I_{SC} will be very close to I_L (i.e., $I_{SC} \approx I_L$). The second parameter is called open circuit voltage (V_{OC}) which represents the voltage across the cell in open circuit condition (I=0). The expression can be written as

$$V_{OC} \approx \frac{AkT}{q} \ln\left(\frac{I_L}{I_0} + 1\right). \qquad (2.9)$$

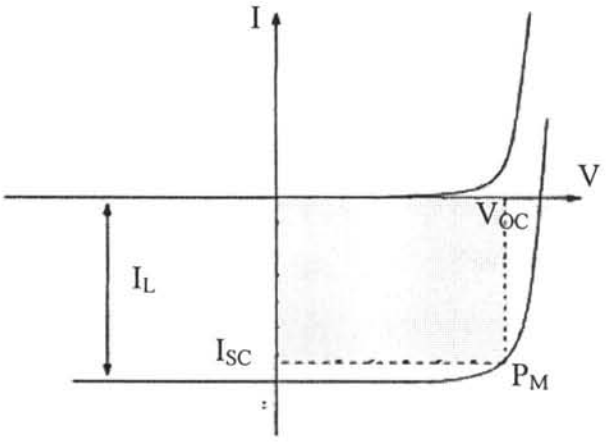

Figure 2.7: I-V characteristic curves

Figure 2.7 shows the I-V characteristic of a typical solar cell under dark and illumination conditions. Therefore, we can then define some of the more important parameters in evaluating solar cells. When a finite load resistance is connected to the solar cell, the power delivered to the load is equal to the product of I and V. In practice, a particular load resistance can be matched such that the power output is maximum. The maximum power output (P_M) is defined as

$$P_M = I_M V_M, \qquad (2.10)$$

where I_M and V_M are the corresponding current and voltage that give maximum output power (the shade area in Fig. 2.7).

The third parameter is fill factor (FF) which can be defined as the following,

$$FF = \frac{P_M}{I_{SC} V_{OC}} = \frac{I_M V_M}{I_{SC} V_{OC}}. \qquad (2.11)$$

The fill factor is affected by series resistance, shunt resistance, and current transport mechanism, which determine the shape of the illuminated I-V characteristics of a solar cell. Ideally, the series resistance should be close to zero. A large series resistance will lead to a decrease in I_{SC} as well as drastic decrease in FF. While an ideal shunt resistance should be as large as possible, a small resistance will result in

small V_{OC} and FF. For cells of reasonable efficiency, it has a value in the range 0.7 to 0.75.

Finally, the most important parameter in evaluating solar cells is the conversion efficiency (η). It is defined as the ratio of the maximum output power to the input power. The expression is given as

$$\eta = \frac{P_M}{P_{in}} = \frac{I_M V_M}{P_{in}} = \frac{FF\ I_{SC} V_{OC}}{P_{in}}, \qquad (2.12)$$

where P_{in} is the incident power of the solar radiation that reaches the surface of solar cell.

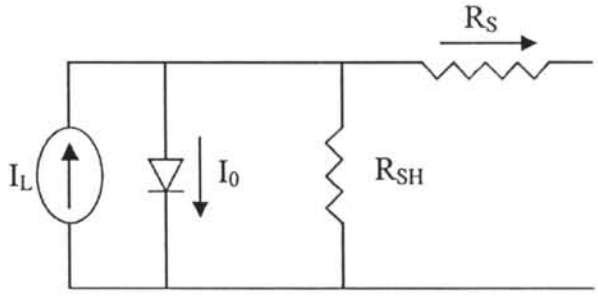

Figure 2.8: Equivalent circuit of p-n junction solar cells [39].

Figure 2.8 shows the equivalent circuit of p-n junction solar cells under illumination. The generation of the photocurrent I_L is represented by a current generator, in parallel with a diode that represents the pn-junction. There are two resistances shown in the figure. R_S represents the resistive loss. This resistive loss is usually due to the sheet resistance of the window, internal resistance of absorber and contact resistance (front and back), which should ideally be zero, but always exists, in a practical solar cell. Since it represents the resistive loss outside the p-n junction, it should be minimized to deliver maximum power to load.

The parallel (or shunt) resistance, R_{SH} represents current loss across the junction due to any parallel paths for the junction current to flow. If the junction defect density is small, R_{SH} is usually large. Ideally, such parallel paths should not exist, making R_{SH} infinite.

2.4.4 Efficiency Limits

In the previous section, three parameters could be used to characterize the performance of solar cells. In this section, the ideal limits of I_{SC} and V_{OC} will be reviewed. The upper limit of I_{SC} can be determined from any selected solar cell material. Under ideal conditions, the incidence of each photon having energy greater than the band gap will give rise to one electron flowing in the external circuit. The maximum I_{SC} is found by integrating spectral distribution from low wavelength up to the maximum wavelength for which electron-hole pairs can be generated for a given semiconductor. As the band gap decreases, the I_{SC} increases as shown in Fig. 2.9.

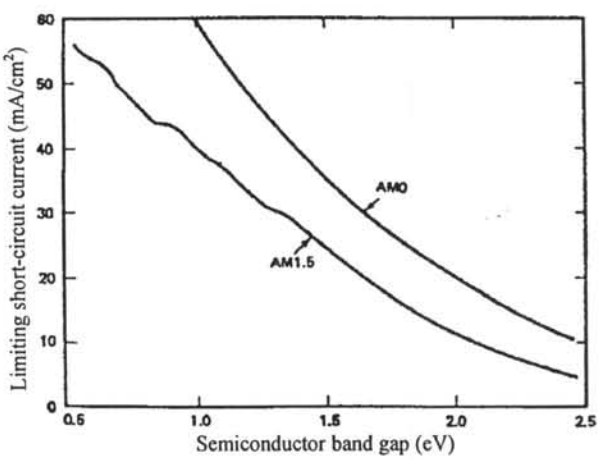

Figure 2.9: Upper limits of the short-circuit current density as a function of the energy band gap of the solar cell material [40].

The limitations of V_{OC} of solar cells are not clearly defined. From the Eq. 2.9, V_{OC} is given by

$$V_{oc} = \frac{AkT}{q} \ln\left[\frac{I_L}{I_0} + 1\right]. \qquad (2.13)$$

I_0 is the diode saturation current calculated as

$$I_0 = \frac{qD_e n_i^2}{L_e N_A} + \frac{qD_h n_i^2}{L_h N_D}, \qquad (2.14)$$

where D_e, D_h are the diffusion coefficients of electron and hole. L_e, L_h are the diffusion length for electron and hole, respectively. n_i is the intrinsic carrier concentration. N_A, N_D are the effective density of state for electron and hole, respectively.

Parameter in Eq. 2.14 which depends on the choice of semiconductor material is n_i^2,

$$n_i^2 = N_C N_V \exp\left[-\frac{E_g}{kT}\right]. \qquad (2.15)$$

Eqs. 2.13 and 2.14 reveals that I_0 needs to be as small as possible for maximum V_{OC}. From the theoretical calculation, the maximum value of V_{OC} decrease with decreasing band gap which opposite from the obtained for I_{SC}. Hence, there will be an optimum band gap for highest efficiency. Combination with the results of maximum I_{SC} allows the maximum energy-conversion efficiency to be calculated as shown in Fig 2.10. The theoretical maximum efficiencies for single junction cells can be achieved with band gap between 1.1 and 1.5 eV for AM 1.5 global radiation.

Theoretical calculations of efficiency for different sun spectra are shown in Fig. 2.10 [41]. It indicates that the optimal band gap of the absorber layer occurs between 1.4 to 1.6 eV. The near-optimal efficiency (29%) for AM1.5 with 1 sun (C=1) irradiation occurs at GaAs (1.4 eV), whereas the peak efficiency for silicon (1.1 eV) of about 26% is lower than optimum but still relatively high [42]. Moreover, the curve of efficiency for AM1.5 with 1000 suns (C=1000) shows the broadening of the optimal band gap between 1.1-1.4 eV.

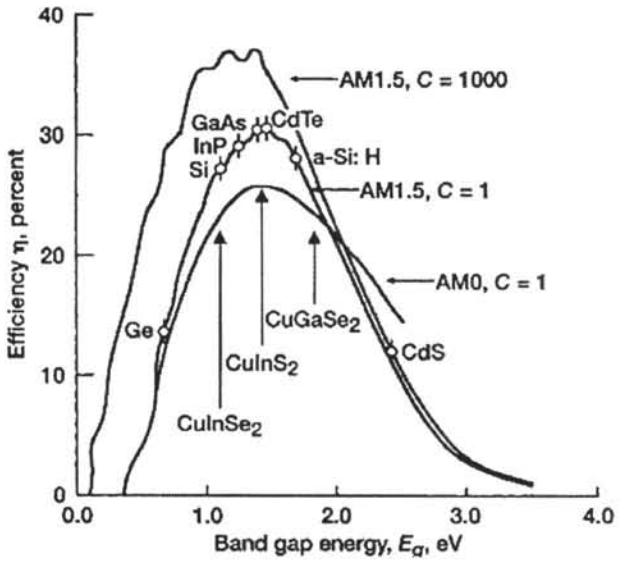

Figure 2.10: Theoretical solar cell efficiency as a function of band gap for spectrum distribution at AM1.5 and AM0 with a power density of 1 sun, and for AM1.5 with 1000 sun (= 844 kW/m^2) [41].

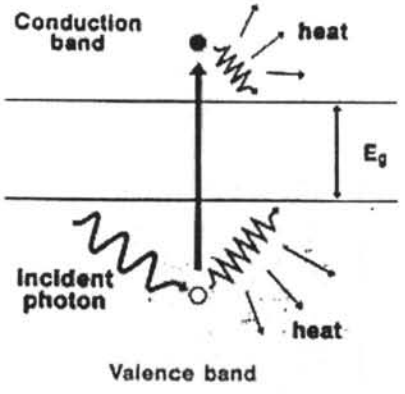

Figure 2.11: The major loss mechanism in solar cells.

Figure 2.11 shows major loss mechanisms in solar cells. In practice, an electron-hole pair created by high-energy photon quickly "thermalizes" or relaxes back to band edge. The energy wasted is dissipated as heat [43].